Structural Characterization of a Three-Disulfide Intermediate of Ribonuclease A Involved in Both the Folding and Unfolding Pathways†

Sekhar Talluri, David M. Rothwarf, and Harold A. Scheraga*

Baker Laboratory of Chemistry, Cornell University, Ithaca, New York 14853-1301

Received April 7, 1994; Revised Manuscript Received June 20, 1994®

ABSTRACT: Earlier studies of the unfolding pathway of native bovine pancreatic ribonuclease A (using dithiothreitol as the reducing agent) revealed that the three-disulfide species lacking the disulfide bond between cysteine 65 and cysteine 72 is the most highly populated intermediate [Rothwarf & Scheraga (1991) *J. Am. Chem. Soc. 113,* 6293–6294]. This unfolding intermediate is referred to as des-[65–72]-RNase A. In order to determine the role of des-[65–72]-RNase A, i.e., of the 65–72 disulfide bond, in the structural folding/unfolding processes of RNase A, the stability and structure of this unfolding intermediate were determined by examining its thermal transition curve and by using two- and three-dimensional homonuclear ^{1}H NMR spectroscopy. The midpoint of the thermal transition of des-[65–72]-RNase A was found to be 17.8 °C lower than that of native RNase A. A set of conformations that are consistent with the NMR-derived constraints was obtained by minimizing, first, a variable-target function and, then, the conformational energy. These conformations exhibit a well-defined structure that is very similar to that of native ribonuclease A in regions where the native protein has a regular backbone structure such as a β-sheet or a helix. Some of the loop regions of the several computed structures exhibit large deviations from each other as well as from native ribonuclease A. However, these results indicate that des-[65–72]-RNase A has a close structural similarity to RNase A in all regions with the only major differences occurring in a loop region comprising residues 60–72. This led to the conclusion that, in reduction pathways that include des-[65–72]-RNase A (at 25 °C, pH 8.0), the rate-determining step corresponds to a partial unfolding event in one region of the protein and not to a global conformational unfolding process. The results further suggest that, in the regeneration pathways involving des-[65–72]-RNase A, the loop region from 60 to 72 is the last to fold.

Disulfide bonds play a critical role in the folding of proteins as well as in the stabilization of native protein structures (Anfinsen & Scheraga, 1975; Richardson, 1981; Thornton, 1981; Creighton, 1988; Doig & Williams, 1991; Kosen, 1992). However, in order to understand this role, it is necessary to study the contribution of individual disulfide bonds. RNase A[1] is one of the best characterized disulfide-containing proteins, in terms of its three-dimensional structure as well as its folding/unfolding pathways (Borkakoti *et al.*, 1982; Wlodawer *et al.*, 1988; Schultz *et al.*, 1992; Konishi & Scheraga, 1980a,b; Konishi *et al.*, 1981, 1882a–c; Scheraga *et al.*, 1984; Rothwarf & Scheraga, 1991, 1993a–d). An early-forming intermediate in the reduction of RNase A by dithiothreitol lacks the 65–72 disulfide bond (Rothwarf & Scheraga, 1991). In order to clarify the role of this disulfide bond in the regeneration/reduction pathways of RNase A, we examined the thermal stability and determined the solution structure of a species lacking this bond, viz., des-[65–72]-RNase A.

Determination of the stability and solution structure of des-[65–72]-RNase A addresses an important issue in the regeneration/reduction pathways of RNase A, *viz.*, the role of des-[65–72]-RNase A in structural folding/unfolding pathways of RNase A. The purpose of studying regeneration/reduction pathways of proteins is to exploit the coupling between conformational changes and disulfide bond formation to trap folding intermediates and then determine their structures in order to elucidate the interresidue interactions that give rise to these intermediates. Therefore, any interpretation of a conformational folding/unfolding pathway depends on knowledge of the stability and structure of the intermediates. Thus, while kinetic studies provide the necessary framework for elucidating regeneration/reduction pathways, straightforward and meaningful interpretations can be achieved only when the stability and structural properties of the intermediates have been determined. This has been clearly evident in studies of bovine pancreatic trypsin inhibitor (BPTI). Determination of the solution structures of all of the well-populated regeneration/reduction intermediates (Naderi *et al.*, 1991; van Mierlo *et al.*, 1991, 1993; Hurle *et al.*, 1992; Darby *et al.*, 1992; Staley & Kim, 1992) has led to a clearer understanding of the folding/unfolding processes of BPTI (Goldenberg, 1992).

† This work was supported by a research grant from the National Institute of General Medical Sciences (GM-24893), National Institutes of Health. Support was also received from the National Foundation for Cancer Research. Some of the computations were carried out at the Cornell National Supercomputer Facility, a resource of the Cornell Theory Center, which receives major funding from the National Science Foundation and the IBM Corporation, with additional support from New York state and members of the Corporate Research Institute.

* Author to whom correspondence should be addressed.

® Abstract published in *Advance ACS Abstracts,* August 1, 1994.

[1] Abbreviations: AEMTS, (2-aminoethyl)methanethiosulfonate; HEPES, *N*-(2-hydroxyethyl)piperazine-*N'*-(2-ethanesulfonic acid); RNase A, bovine pancreatic ribonuclease A; des-[65–72]-RNase A, RNase A lacking the 65–72 disulfide bond; DSS, 2,2-dimethyl-2-silapentane-5-sulfonate; Tris, tris(hydroxymethyl)aminomethane; COSY, two-dimensional correlation spectroscopy; DQF-COSY, two-dimensional double-quantum-filtered correlation spectroscopy; TOCSY, two-dimensional total correlation spectroscopy; NOESY, two-dimensional nuclear Overhauser effect spectroscopy; TOCSY–NOESY, three-dimensional experiment combining two-dimensional total correlation and nuclear Overhauser effect spectroscopy; DIANA, distance geometry algorithm for NMR applications; REDAC, redundant dihedral angle constraint; ECEPP, empirical conformational energy program for peptides.

0006-2960/94/0433-10437$04.50/0

The existence of des-[65–72]-RNase A in the reduction pathways of RNase A is well established. Reduction studies of RNase A by reduced dithiothreitol at pH 8, 15–25 °C, indicate that des-[65–72]-RNase A is the major reduction intermediate populated during the reduction of RNase A (Rothwarf & Scheraga, 1991; Y.-J. Li, D. M. Rothwarf, and H. A. Scheraga, unpublished results). A detailed kinetic analysis of the reduction process by reduced dithiothreitol at 25 °C, pH 8.0 (D. M. Rothwarf and H. A. Scheraga, unpublished results) indicates that des-[65–72]-RNase A is reduced about 5 times more rapidly than is native RNase A through pathways other than the one involving formation of des-[65–72]-RNase A and that the rate-determining step in reduction pathways involving formation of des-[65–72]-RNase A is the cleavage of the 65–72 disulfide bond. It is important to emphasize that, while the rate of reduction of des-[65–72]-RNase A is about 5 times more rapid than its formation, its rate of reduction is approximately 5 orders of magnitude slower (D. M. Rothwarf and H. A. Scheraga unpublished results) than the average rate of disulfide reduction in the disordered intermediates observed during the regeneration of RNase A (Rothwarf & Scheraga, 1993b) or than the rate of reduction of oxidized glutathione by dithiothreitol (Rothwarf & Scheraga, 1992). This indicates that a substantial activation barrier exists between des-[65–72]-RNase A and the completely unfolded state.

Des-[65–72]-RNase A is formed in one of the two major regeneration pathways populated at 25 °C, pH 8, when oxidized dithiothreitol is used as the oxidizing agent. The majority of three-disulfide intermediates populated during regeneration are largely conformationally disordered, are in rapid equilibrium with each other, and have little or no enzymatic activity (Rothwarf & Scheraga, 1993a,b). On the other hand, des-[65–72]-RNase A corresponds to a species that appears after the rate-determining step in folding, is not in rapid equilibrium with the other three-disulfide species (D. M. Rothwarf and H. A. Scheraga unpublished results), and, as reported here, has 81% of the enzymatic activity of native RNase A.

An additional property of des-[65–72]-RNase A determined from earlier studies is that one or both cysteines in des-[65–72]-RNase A may be partially buried and/or that a significant conformational change occurs upon cleavage of the 65–72 disulfide bond. This conclusion is based on the experimental observation that des-[65–72]-RNase A cannot be blocked effectively by iodoacetate (Rothwarf & Scheraga, 1991). The ability to block des-[65–72]-RNase A with AEMTS [which reacts about 10^5 times more rapidly with thiols than does iodoacetate (Rothwarf & Scheraga, 1991)], however, indicates that both cysteine residues become exposed through either local or global fluctuations in the protein within the 2-min blocking time.

Des-[65–72]-RNase A represents an unusual species in that it appears after the rate-determining step in *both* reduction and regeneration under the conditions normally used in those experiments. The structural characterization presented here will help explain the role of des-[65–72]-RNase A in the folding/unfolding pathways of the protein.

In addition to the information to be obtained about regeneration/reduction pathways of RNase A, the thermal denaturation and NMR studies of AEMTS-blocked des-[65–72]-RNase A presented here will explain the contribution made by the 65–72 disulfide to the stability and structure of the native protein. While it is generally accepted (Poland & Scheraga, 1965; Anfinsen & Scheraga, 1975; Lin *et al.*, 1984; Pace *et al.*, 1988; Doig & Williams, 1991; Cooper *et al.*, 1992) that the major contribution of disulfide bonds is the stabilization of the native protein through destabilization of the denatured state, there is also evidence that disulfide bonds directly affect the stability and dynamics of the native state of a protein (Kosen, 1992; Kuroki *et al.*, 1992). Since X-ray crystallographic studies of RNase A (Borkakoti *et al.*, 1982) have shown that residues 61–64 and 71–75 of RNase A form two strands of a four-strand antiparallel β-sheet, it seems likely that the removal of the 65–72 disulfide bond would cause a disruption of the structure of that antiparallel β-sheet, possibly resulting in longer-range effects on the structure of the protein.

MATERIALS AND METHODS

RNase A (Sigma Type IA) was purified as described by Rothwarf and Scheraga (1993a). AEMTS was synthesized as described by Bruice and Kenyon (1982). Ultrapure reduced dithiothreitol was obtained from Boehringer-Mannheim. All other reagents were of the highest grade commercially available.

Preparation and Purification of Des-[65–72]-RNase A. Des-[65–72]-RNase A was prepared by reducing RNase A (0.35–2.0 mM) with 20 mM reduced dithiothreitol, in 100 mM Tris and 2 mM EDTA, pH 8.0, at 25 °C under a steady stream of humidified argon. After 24–32 h, the sample was blocked by addition of a 3–5-fold excess (over the thiol concentration) of AEMTS freshly dissolved in Tris buffer, pH 8.0. After 5 min, the blocked protein was desalted on an HR16/50 column (Pharmacia) packed with G-25 superfine resin (Pharmacia) into 50 mM triethylammonium acetate, pH 5.0. An LKB 2150 pump and an Isco UA-5 detector with a Type 9 optical unit and 280-nm filters constituted the solvent delivery and detection system.

Disulfide-blocked des-[65–72]-RNase A was purified on a Rainin Hydropore SCX 21 × 10-cm column in 25 mM HEPES and 1 mM EDTA, pH 7.0, using a linear gradient from 0 to 150 mM NaCl in 100 min at a flow rate of 8.6 mL/min. An LKB 2249 gradient system with an Isco UA-5 detector with Type 9 optical unit and 280-nm filters was used. The chromatographic separation was similar to that shown in Figure 2 of Rothwarf and Scheraga (1991).

The identity of the broken disulfide bond in des-[65–72]-RNase A was confirmed by chymotryptic/tryptic digestion followed by disulfide-specific peptide mapping, and amino acid analysis. A detailed discussion of the procedures that were used for peptide mapping will be published elsewhere (D. M. Rothwarf and H. A. Scheraga unpublished results). Hereafter, "des-[65–72]-RNase A" refers to the AEMTS-blocked species.

Activity Measurements. The activities of des-[65–72]-RNase A and native RNase A were assayed as described by Rothwarf and Scheraga (1993d) except that the assay buffer corresponded to that used in the thermal transition studies, *viz.*, 50 mM sodium acetate, pH 4.6. Results are given in the last column of Table 1.

Thermal Transition. Des-[65–72]-RNase A and native RNase A were dissolved in 50 mM sodium acetate, pH 4.6, at concentrations of 17 and 11 μM, respectively. All absorbance measurements were made on a modified Cary 14 spectrophotometer (Denton *et al.*, 1982) connected to a Sun IPC computer. The protein concentration was determined by using the value of 9300 M^{-1} cm^{-1} at 275 nm for the extinction coefficient of both the native protein (Konishi & Scheraga, 1980a) and des-[65–72]-RNase A. The thermal transition was followed by measuring the absorbance at 287 nm in a

Table 1: Properties of Unmodified RNase A and Des-[65–72]-RNase A at pH 4.6

protein	T_m (°C)	$\Delta H°$ (T_m) (kcal/mol)	$\Delta S°$ (T_m) (eu)	$\Delta\mu°_{conf}$[a] (kcal/mol)	activity[b]
native RNase A	56.2 ± 0.4[c]	106.7 ± 8.7	324 ± 26	2.7 ± 0.2	100
Des-[65–72]-RNase A	38.4 ± 0.4[c]	80.3 ± 8.0	258 ± 24	−2.4 ± 0.2	81 ± 6

[a] Determined at 47.3 °C. [b] Enzymatic activity relative to that of the unmodified native protein at 15 °C. [c] The error is calculated at the 95% confidence limit.

1-cm path length cell in a thermoregulated block connected to a computer-interfaced Neslab RTE-110 bath. The temperature of the block was measured by a thermocouple inserted into a buffer-containing cell located in a second cell compartment of the block. The protein solutions were equilibrated for 15 min at each temperature. In order to minimize the continuous length of time that solutions were held at or above the transition temperature, solutions were taken up and back rapidly through the entire range of temperature four separate times. This also served to minimize effects due to instability of the spectrophotometer. A control experiment in which the change in absorbance at 287 nm was followed as a function of temperature for the sample cell containing only buffer showed that the buffer and the cell made no contribution to the measured thermal transitions.

NMR Spectroscopy. Samples of des-[65–72]-RNase A for studies in H_2O were prepared by dissolving the protein in 90% H_2O/10% D_2O and then adjusting the pH to 4.6 ± 0.15 using dilute HCl and NaOH. The final concentration of the protein in this solution was approximately 1–2 mM. Studies in D_2O were carried out at a protein concentration of about 0.8 mM at pH 4.6. The pH in D_2O is reported without any correction for the deuterium isotope effect on the observed pH (pD). All samples contained 0.1 mM DSS.

All NMR experiments were carried out on a Varian Unity-500 spectrometer.

The following two-dimensional NMR experiments were carried out in H_2O at 20 °C: DQF-COSY (Piantini *et al.*, 1982), NOESY (Jeener *et al.*, 1979; Macura & Ernst, 1980), and TOCSY (Braunschweiler & Ernst, 1983; Bax & Davis, 1985). For the DQF-COSY experiment, 1024 increments were acquired. For the NOESY experiment in H_2O, at 20 °C, a mixing time of 150 ms was used and 600 increments were acquired. TOCSY spectra were acquired with mixing times of 40 and 51 ms. The shorter value of the mixing time (40 ms) in the TOCSY experiment enhances the peaks between resonances that are directly coupled to each other, and longer mixing times are used to emphasize cross peaks due to relayed transfer of magnetization. A 1.5-ms purging pulse was used before and after the mixing time to remove the contributions from zero-quantum coherence.

In addition to the spectra at 20 °C, DQF-COSY, TOCSY, and NOESY spectra were also obtained at 15 °C. Mixing times of 75 and 125 ms were used for the NOESY spectra acquired at 15 °C. The large signal from water was suppressed by using low-power irradiation resonant with the water frequency. A total of 512 increments were collected for DQF-COSY and NOESY spectra, and 410 increments were collected for the TOCSY spectra.

In addition, the following spectra of des-[65–72]-RNase A in D_2O were obtained at 15 °C: DQF-COSY, TOCSY with a mixing time of 55 ms, and NOESY with a mixing time of 100 ms. Another DQF-COSY spectrum was acquired at 10 °C for additional studies of slowly exchanging backbone amide hydrogens. The number of increments was 512 for these experiments in D_2O.

A total of 4096 points were collected for each increment for all of the 2D spectra of des-[65–72]-RNase A.

For comparison purposes, a 4 mM solution of native RNase A was prepared by dissolving the appropriate amount of lyophilized RNase A in 90% H_2O and 10% D_2O. DSS was added as a reference for chemical shifts. The pH was adjusted to 4.6. NOESY and TOCSY spectra of native RNase A were obtained at 15 °C. A total of 2048 points were acquired for each increment for the NOESY and TOCSY experiments. Eight hundred ninety increments were acquired for the NOESY and 594 increments were acquired for the TOCSY experiment.

Three-dimensional TOCSY–NOESY (Griesinger *et al.*, 1989; Oschkinat *et al.*, 1989) spectra of des-[65–72]-RNase A were recorded in H_2O and in D_2O at pH 4.6 and 15 °C. An eight-step phase cycle was used to select the appropriate coherence and to cancel artifacts due to imperfections in the quadrature detection system. Pure absorption line shapes were obtained in the *F*1 dimension by using time-proportional phase incrementation (Redfield & Kunz, 1975). The NOESY mixing time in the TOCSY–NOESY experiment in D_2O was 100 ms, and the TOCSY mixing time was 45 ms. For the experiment in H_2O, a NOESY mixing time of 150 ms and a TOCSY mixing time of 45 ms were used.

The total experiment time required for each 2D experiment was 1–2 days. For each 3D experiment, the time required was approximately 5 days.

NMR data were processed by using the software programs NMR2, Ftnmr, and Felix for computing the Fourier transforms and for plotting and displaying the data. In addition, the software program EASY (Eccles *et al.*, 1991) was also used for displaying data on the computer screen.

The range of three-dimensional structures that are consistent with NMR-derived constraints was determined by using the program DIANA (Güntert *et al.*, 1991a,b; Güntert & Wüthrich, 1991). We have updated the geometry of the amino acid residues used by DIANA, so that the geometry of all amino acid residues is identical to that used in the ECEPP/3 force field (Némethy *et al.*, 1992). The DIANA computations were carried out with a Sun IPX workstation, a Titan Stardent 3000 workstation, a cluster of IBM RS-6000's, an IBM ES9000 supercomputer, and a parallel computer from Kendall Square Research (KSR). It was ncessary to make some minor changes in the program for implementation on the parallel computer (KSR), but we checked that the results from the KSR were similar to those obtained on other machines; it is not possible to obtain identical results on all computers even if the same program and the same input data are used. This is because of small differences in the precision of numerical computations on computers with different architectures (Güntert & Wüthrich, 1991). Random conformations were generated and a variable-target function was minimized on all of the computers mentioned above. Different computers report slightly different values of the target function for the *same* conformation (Güntert & Wüthrich, 1991). Therefore, to compare conformations whose variable-target functions were minimized on different computers, we collected all of the *minimized* conformations on the Sun computer and reevaluated the target function for each of these minimized conformations.

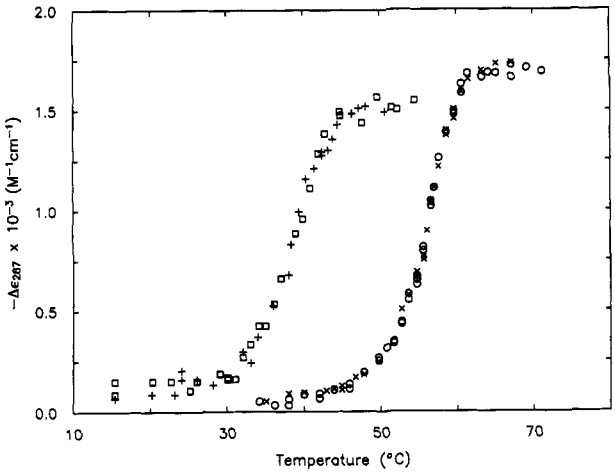

FIGURE 1: Thermal transition curves for des-[65–72]-RNase A (□, heating; + cooling) and native RNase A (○, heating; ×, cooling) in 50 mM sodium acetate, pH 4.6.

Restrained energy minimization was carried out as described earlier (Montelione *et al.*, 1992).

RESULTS AND DISCUSSION

Thermal Transition. The reversible thermal transition curves of native RNase A and des-[65–72]-RNase A are shown in Figure 1. Scatter in the data is due primarily to instabilities of the spectrophotometer rather than to any thermally induced modifications (the protein used in the thermal transitions had the same activity before and after the measurements of the thermal transition and was homogeneous by cation-exchange HPLC analysis). Thermodynamic parameters obtained from van't Hoff plots derived from the curves in Figure 1 are given in Table 1. The reversible thermal transition of unmodified RNase A has been studied extensively (Hermans & Scheraga, 1961; Scott & Scheraga, 1963; Brandts & Hunt, 1967; Tsong *et al.*, 1970; Privalov *et al.*, 1973; Tiktopulo & Privalov, 1974; Lin *et al.*, 1984). The value of $\Delta H(T_m)$ determined here is in excellent agreement with the values determined by Privalov *et al.* (1973) by calorimetric and optical methods at pH 4.0 (between 99 and 108 kcal/mol) and within the range of the calorimetric values of $\Delta H_{cal}(T_m)$ and $\Delta H_{vH}(T_m)$ (126 and 64 kcal/mol, respectively) measured calorimetrically at pH 4.0 (Tsong *et al.*, 1970).

The thermodynamic properties listed in Table 1 indicate that the disruption of the 65–72 disulfide bond has decreased the thermal stability of the protein. This difference can be expressed quantitatively by means of the conformational chemical potential difference, $\Delta\mu^{\circ}_{conf}$, between the native and unfolded conformations of des-[65–72]-RNase A and native RNase A, respectively. $\Delta\mu^{\circ}_{conf}$ was introduced by Konishi *et al.* (1982b) to compare species which differ slightly in their chemical composition. $\Delta\mu^{\circ}_{conf}$ depends only on the conformation of the protein molecule. $\Delta\mu^{\circ}_{conf}$ as used here is equivalent to the free energy of unfolding. The values of $\Delta\mu^{\circ}_{conf}$ for des-[65–72]-RNase A and for native RNase A, respectively, were calculated by using van't Hoff plots obtained from the data shown in Figure 1. The value of $\Delta\mu^{\circ}_{conf}$ at 47.3 °C (the temperature midway between the T_m's) was found to be −2.4 kcal/mol for des-[65–72]-RNase A and 2.7 kcal/mol for native RNase A. This means that, at 47.3 °C, the native protein is largely folded whereas des-[65–72]-RNase A is largely unfolded.

The errors in the thermodynamic parameters listed in Table 1 include the error in the baseline slopes used in the van't Hoff analysis and, in the case of $\Delta\mu^{\circ}_{conf}$, the errors in the values of T_m. The errors given for $\Delta\mu^{\circ}_{conf}$ at 47.3 °C are likely to be larger than the ±0.2 kcal/mol listed in Table 1 because these errors reflect only random error and do not account for systematic errors arising from the extrapolation to 47.3 °C, especially contributions arising from heat capacity factors. No attempt has been made here to account for these systematic errors since it is $\Delta\Delta\mu^{\circ}_{conf}$ that is the thermodynamic quantity of interest and, by evaluating $\Delta\Delta\mu^{\circ}_{conf}$ at a temperature exactly midway between the T_m's of the two proteins, these systematic errors should for the most part cancel (Denton & Scheraga, 1991) so that ±0.4 kcal/mol should be an accurate reflection of the error in $\Delta\Delta\mu^{\circ}_{conf}$.

If we assume that the folded conformation of des-[65–72]-RNase A and native RNase A have the same value of μ°_{conf}, then $\Delta\Delta^{\circ}_{conf}$ can be attributed to the difference in the properties of the denatured states of the two proteins. This value of 5.1 kcal/mol can be compared to an estimate of the difference in the free energies of the two denatured proteins due to a difference in loop entropy between the two species by using a model of overlapping and dependent loops (Wang & Uhlenbeck, 1945; Poland & Scheraga, 1965) as described by Lin *et al.* (1984). The free energy difference between the two species due to loop entropy was calculated to be 3.9 kcal/mol at 47.3 °C. This is 1.2 kcal/mol less than the experimental value of $\Delta\Delta\mu^{\circ}_{conf}$ and well outside the experimental error of ±0.4 kcal/mol. It is important to remember that the loop entropy calculation relies on the assumption of the applicability of a Gaussian distribution to short chains and is therefore only an approximation. Therefore, the observed difference in the calculated value of the loop entropy and the observed value of $\Delta\Delta\mu^{\circ}_{conf}$ might be due only to the approximations made in the loop entropy calculation. If the loop entropy calculations are accurate, it would imply that there is an additional enthalpic or entropic contribution to $\Delta\Delta\mu^{\circ}_{conf}$. This could be due to electrostatic repulsion between the two charged blocking groups at the end of the cysteamine residues in des-[65–72]-RNase A or to disruption of the hydrogen bond involving Lys-66 and Asp-121 (see the section on backbone hydrogen–deuterium exchange). Enthalpic effects in loop formation have been demonstrated for the 65–72 loop (Milburn & Scheraga, 1988; Altmann & Scheraga, 1990).

Identification of Spin Systems and Sequential Resonance Assignments. Before beginning *sequential* resonance assignments, we identified 67 out of the 124 spin systems (54%) from TOCSY and DQF-COSY spectra, by using the procedure described earlier (Robertson *et al.*, 1989).

Sequential resonance assignments for the ^1H resonances of des-[65–72]-RNase A were obtained by the same procedure that was used earlier for assignment of the resonances of native RNase A (Robertson *et al.*, 1989; Rico *et al.*, 1989). Briefly, the procedure is a combination of the strategy described by Wüthrich *et al.* (Billeter et al., 1982; Wüthrich *et al.*, 1982, 1984; Wüthrich, 1986) and that described by Englander and Wand (1987). In the strategy described by Wüthrich *et al*, the cross peaks in *J*-correlated spectra are classified into spin systems, and these spin systems are subsequently assigned a unique place in the sequence using sequential connectivities observed in the NOE spectrum. In the strategy described by Englander and Wand, assignment starts with a search for NH–C^{α}H–C^{β}H *J*-coupled units. These units are then arranged in a certain order using the distinct NOE patterns characteristic of helices, β-sheets, turns, and extended chains. Finally, the recognition of a few amino acid side-chain types is used to assign a unique place for these arranged units within

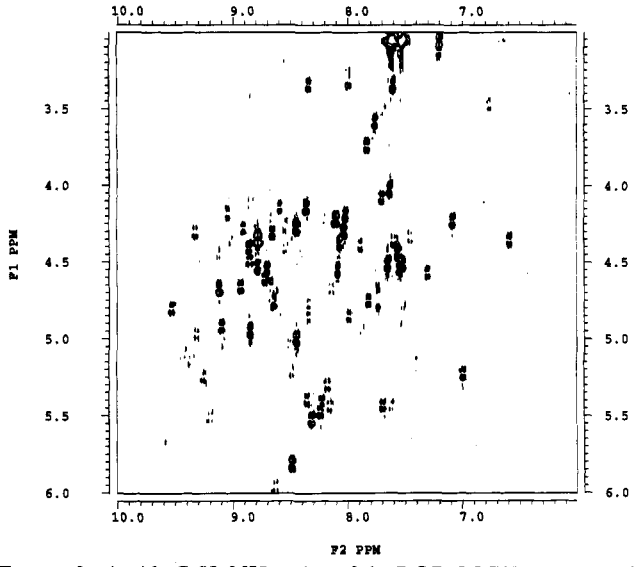

FIGURE 2: Amide $C^{\alpha}H$–NH region of the DQF-COSY spectrum of des-[65–72]-RNase A in H_2O at pH 4.6 and 20 °C.

the polypeptide sequence. The strategy of Englander and Wand is particularly useful when more than one C^{α} proton has the same chemical shift—a phenomenon that occurs quite frequently in des-[65–72]-RNase A.

Using this combined assignment strategy, we were able to obtain assignments for the backbone amide NH's and $C^{\alpha}H$'s for residues 1–40, 42–59, 61–64, 66–79, 81–119, and 121–124. The amino acid residues without backbone assignments at this stage are Lys-41, Gln-60, Cys-65, Ser-80, and Phe-120. The amide NH of Lys-41 was tentatively assigned to 7.26 ppm by using an NOE to the amide NH of Cys-40. We were unable to confirm this assignment by using $C^{\alpha}H$–NH or $C^{\beta}H$–NH NOE's because the $C^{\beta}H$ of Cys-40 has the same chemical shift as that of Tyr-76; in addition, the $C^{\alpha}H$ chemical shift of Cys-40 is 4.77 ppm, almost identical to that of H_2O. We were unable to find a TOCSY or COSY peak with an amide NH peak at 7.26 ppm (Figure 2). Therefore, this assignment is only tentative and might have to be revised in the future if additional data such as ^{15}N-resolved three-dimensional spectra are acquired. The $C^{\alpha}H$ and $C^{\beta}H$ of Ser-80 could be assigned at the end of the sequential resonance assignment because the $C^{\alpha}H$–$C^{\beta}H$ cross peak occurs in a characteristic part of the DQF-COSY spectrum. The only unassigned cross peak in this region was assigned to $C^{\alpha}H$–$C^{\beta}H$ of Ser-80. The chemical shift of the $C^{\alpha}H$ proton of Ser-80 was found to be 4.85 ppm; i.e., it is identical to that of H_2O. We used radio frequency irradiation at 4.8 ppm to saturate the H_2O signal for the NOESY experiment in H_2O. This irradiation saturated the $C^{\alpha}H$ of Ser-80 and made it invisible in the NOESY spectrum. Therefore, we were unable to identify the chemical shift of the amide NH of Ser-80. The $C^{\alpha}H$ of His-119 was well resolved, but we were unable to locate the sequential His-119–Phe-120 $C^{\alpha}H$–NH peak. We were unable to locate the sequential NOE's that are necessary for the assignment of any of the protons of Gln-60. Therefore, Gln-60 remains unassigned in this work.

We obtained tentative assignments for the amide NH and $C^{\alpha}H$ resonances of Cys-65 by using sequential NOE's to Lys-66 and Ala-64; however, we were unable to locate the corresponding $C^{\alpha}H$–$C^{\beta}H$ peak in the DQF-COSY spectrum. Therefore, in this work, the assignments for the amide NH and $C^{\alpha}H$ resonances of Cys-65 remain tentative. We were unable to obtain assignments for the AEMTS blocking groups of Cys-72 and Cys-65 because we were unable to find any NOE connectivities from the resolved amide NH or $C^{\alpha}H$ resonances of Cys-72. Cys-65 occurs in a crowded part of the spectrum. Therefore it was not possible to identify the NOE's that might belong to the side chain of Cys-65.

The $C^{\delta}H$–$C^{\epsilon}H$ peaks of histidines could be differentiated readily from those of other spin systems because of their unique chemical shifts. There are four histidines in des-[65–72]-RNase A; therefore, we expect four cross peaks in this region. However, we found only three of the four $C^{\delta}H$–$C^{\epsilon}H$ cross peaks. These peaks were assigned to His-48, His-105, and His-119 by using the $C^{\beta}H$–$C^{\delta}H$ NOE's after the $C^{\beta}H$'s were assigned by using the sequential resonance assignment procedure. A cross peak at $F_2 = 7.64$, $F_1 = 7.95$ ppm was found that could possibly be assigned to His-12. However, the chemical shifts are quite different from those expected for His-12. This cross peak could not be assigned because it does not show any NOE connectivities. The side-chain His-12 $C^{\delta}H$–$C^{\epsilon}H$ cross peak could not be identified, either because of chemical shift overlap or because the intensity of the cross peak is reduced due to conformational chemical exchange.

Many of the assignments that were obtained by using data from the two-dimensional NMR experiments were confirmed by using the data from the three-dimensional TOCSY–NOESY experiment.

At the end of the sequential resonance assignment procedure, 120 of the 124 spin systems were assigned (98%).

The chemical shifts of des-[65–72]-RNase A at 15 °C are presented in Table 2.

Measurement of Backbone Amide $^3J_{HN-C^{\alpha}H}$ Coupling Constants. In small proteins (<50 residues), the line widths of ^1H resonances are small compared to the $^3J_{HN-C^{\alpha}H}$ coupling constants. Therefore, $^3J_{HN-C^{\alpha}H}$ coupling constants can be estimated from the observed separation of the antiphase components of the doublets in COSY spectra. In des-[65–72]-RNase A, the line widths of the amide NH proton resonances are considerably larger than the expected values of the NH–$C^{\alpha}H$ coupling constants. Therefore, the observed distance between the components of the antiphase doublets in COSY spectra is expected to be larger than the actual coupling constant for proteins of this size (Neuhaus *et al.*, 1985). To overcome this problem, the backbone NH–$C^{\alpha}H$ coupling constants were measured by using the method described by Ludvigsen *et al.* (1991).

The coupling constants were divided into three classes, >8.8 Hz, 5.8–8.8 Hz, and <5.8 Hz. If the measured coupling constant was greater than 8.8 Hz, then the backbone dihedral angle ϕ was restricted to the range −160.0° to −80.0° (Ludvigsen *et al.*, 1991). If the coupling constant was less than 5.8 Hz, then ϕ could be in the range −90° to −30.0°, or it could have a positive value. These two possibilities were distinguished by examining the intensity of the $C^{\alpha}H$–NH NOE. If the coupling constant is less than 5.8 Hz, then the intensity of the $C^{\alpha}H$–NH NOE peak is expected to be much higher for positive values of ϕ than for negative values of ϕ (Ludvigsen *et al.*, 1991).

We were able to obtain constraints on ϕ for 17 amino acid residues that have well-resolved peaks in the DQF-COSY spectrum. The $^3J_{HN-C^{\alpha}H}$ coupling constants for residues Val-47, Glu-49, Ile-81, Cys-84, Lys-98, Thr-100, Lys-104, Ile-107, Ala-109, and Val-116 were found to be greater than 8.8 Hz; consequently, the backbone dihedral angle ϕ for these residues was restricted to the range −160.0° to −80.0°. The $^3J_{HN-C^{\alpha}H}$ coupling constant for residues Gln-11, Met-29, Lys-31, Val-54, Gln-55, Ala-56, and Val-58 were found to be less than 5.8 Hz and the $C^{\alpha}H$–NH NOE was relatively weak;

Table 2: ^{1}H Assignments for Des-[65–72]-RNase A at pH 4.6 and 15 °C

residue	NH	C$^\alpha$H	C$^\beta$H	C$^\gamma$H	C$^\delta$H,C$^\epsilon$H,C$^\zeta$H	residue	NH	C$^\alpha$H	C$^\beta$H	C$^\gamma$H	C$^\delta$H,C$^\epsilon$H,C$^\zeta$H
K 1		4.04	2.00			V 63	8.13	4.22	1.88	0.76, 0.61	
E 2	8.82	4.52	1.94, 2.09			A 64	8.40	4.14	1.29		
T 3	8.59	4.41	4.77	1.45		C 65[a]	8.18	4.57			
A 4	9.08	4.20	1.56			K 66	8.51	4.26	1.81		
A 5	8.96	4.28	1.47			N 67	8.69	4.55	2.91		
A 6	8.05	4.19	1.62			G 68	8.37	(4.12, 3.80)			
K 7	8.86	4.06	2.03			Q 69	8.07	4.53	2.11	2.40	
F 8	8.07	4.47	3.50, 3.17		7.03, 6.87	T 70	8.65	4.70	4.57	1.21	
E 9	7.98	3.78	2.35			N 71	8.51	5.07	3.78		
R 10	8.41	4.24	2.04			C 72	8.43	5.39	3.02, 2.69		
Q 11	8.61	3.82	1.55			Y 73	9.42	5.18	2.89, 2.18		6.69, 6.78
H 12	7.88	4.95	2.74, 1.79			Q 74	9.61	5.65	1.62	2.56	
M 13	8.18	5.45	2.80			S 75	9.05	4.80	4.02		
D 14	8.89	5.02	2.18			Y 76	8.80	4.69	2.98, 3.31		7.26, 6.93
S 15	9.04	4.36	3.81			S 77	9.14	4.94	3.99, 3.79		
S 16	8.10	4.38	3.97, 3.95			T 78	8.38	3.33	3.63	0.70	
T 17	7.58	4.55	4.19	1.11		M 79	8.69	4.60	1.72		
S 18	8.71	4.32	3.84			S 80[a]		4.85	4.12		
A 19	7.64	3.32	1.04			I 81	9.22	5.52	1.76	0.87	
A 20	7.71	3.51	0.90			T 82	9.43	5.15	3.91	1.36	
S 21	8.07	4.30	3.98, 3.82			D 83	9.31	5.03	2.63, 2.53		
S 22	7.78	4.73	4.15, 3.97			C 84	8.77	5.96	3.01, 2.57		
S 23	9.16	4.45	4.16, 4.07			R 85	8.31	5.47	2.00, 1.87		
N 24	8.47	5.02	2.95, 2.72			E 86	8.76	4.26	2.36, 2.15		
Y 25	7.73	4.07	2.95, 3.47		7.18, 6.52	T 87	8.14	4.53	4.56	1.10	
C 26	7.88	3.87	3.20, 2.16			G 88	8.92	3.94			
N 27	8.11	4.55	2.90			S 89	7.67	4.52	3.87, 3.82		
Q 28	7.65	4.03	1.92			S 90	7.02	3.96	3.27, 3.15		
M 29	8.53	4.22	0.92			K 91	7.61	4.45	1.74		
M 30	8.77	4.23	1.71			Y 92	9.43	3.81	3.50, 3.50		6.89
K 31	6.58	4.36	1.93			P 93		3.29	1.14	1.91, 1.78	3.63, 3.47
S 32	8.71	4.20	3.99, 3.90			N 94	8.85	4.95	2.75		
R 33	7.88	4.48	1.86			C 95	7.65	4.70	2.96		
N 34	8.00	4.89	3.17, 2.97			A 96	8.33	4.78	1.22		
L 35	8.15	4.68	2.02	1.57	0.91, 0.77	Y 97	9.47	4.90	2.37		7.03, 6.51, 6.43
T 36	7.71	5.45	4.87	1.21		K 98	9.55	4.81	1.94, 1.80		
K 37	7.10	4.22	1.77			T 99	9.28	5.24	4.26	1.33	
D 38	8.91	4.44	2.72, 2.59			T 100	8.94	4.68	4.15	1.26	
R 39	7.77	3.60	1.71, 1.50	1.37, 1.06	3.07	Q 101	9.11	5.06	1.99		
C 40	9.13	4.77	2.99, 2.81			A 102	9.14	4.67	1.34		
K 41[a]	7.26	4.54	1.64			N 103	8.52	5.82	2.59, 2.31		
P 42		4.61	2.50, 2.14	2.27, 2.19	4.07, 3.96	K 104	8.62	4.79	1.43		
V 43	7.09	5.33	2.11	1.00		H 105	9.30	4.46	3.31, 3.17		8.78, 7.47
N 44	8.76	4.99	2.14			I 106	8.41	5.06	1.81	1.03	
T 45	7.40	5.17	2.35	0.77		I 107	8.21	5.32	1.47	0.68	
F 46	9.26	4.93	2.63		6.80, 6.96, 6.62	V 108	9.18	4.93	2.09	0.80, 0.62	
V 47	9.31	4.31	2.50	1.02, 0.90		A 109	8.36	5.54	1.35		
H 48	9.25	5.36	3.09, 3.50		6.82, 6.80, 8.28	C 110	8.52	5.22	2.64, 1.03		
E 49	6.91	4.89	1.43			E 111	8.75	4.61	2.01, 1.92	2.36	
S 50	9.65	4.29	4.09, 4.28			G 112	8.85	(4.56, 3.80)			
L 51	8.90	4.11	1.79	1.47	1.11, 0.96	N 113	7.87	4.76	2.90, 2.61		
A 52	8.64	4.14	1.41			P 114		4.66	2.34, 1.89		
D 53	7.93	4.39	3.02			Y 115	8.58	4.27	2.99, 2.82		7.18, 6.80
V 54	7.86	3.75	2.20	1.10, 1.06		V 116	7.53	4.85	2.11	0.70, 0.81	
Q 55	9.21	3.64	2.29, 2.77			P 117		4.37	1.05, 0.11	1.07, 1.58	3.61
A 56	7.73	4.08	1.50			V 118	8.88	4.46	2.12	0.81, 0.55	
V 57	7.59	3.01	2.14	0.70, 1.11		H 119	7.63	5.49	3.27, 3.16		7.04, 8.69
C 58	6.77	3.48	2.59, 2.77			F 120[a]		4.40	2.39		6.67, 7.03
S 59	7.54	4.51	4.06, 3.88			D 121	8.60	4.72	2.31, 2.10		
Q 60						A 122	7.37	4.53	1.33		
K 61	7.46	4.35	2.14			S 123	8.24	5.39	3.87, 3.81		
N 62	9.09	4.14	2.68, 2.58		6.71, 6.35	V 124	8.76	4.34	2.04	0.80	

[a] Not unambiguously determined.

therefore, the value of the dihedral angle ϕ was restricted to the range −90° to −30.0° for these residues. These dihedral angle ranges are consistent with the structure of native RNase A.

Backbone Amide Hydrogen–Deuterium Exchange. In D_2O solution, the amide NH protons of most peptides exchange rapidly with the solvent deuterons. In proteins, the rate of H/D exchange can be considerably slower than that in peptides, because the rate of exchange is slowed down due to lack of accessibility to solvent (Richards, 1979; Tuchsen & Woodward, 1985) or to the presence of hydrogen bonds (Kossiakoff, 1982). In addition, the rate of H/D exchange also depends on the extent of internal fluctuations in the protein (Wagner, 1983) as well as on the overall stability of the protein (Wagner *et al.*, 1979a,b). The rate of H/D exchange is also influenced by the local electrostatic field from nearby charged groups (Matthew & Richards, 1983; Delepierre *et al.*, 1987). Because of the large number of factors that contribute to the rate of H/D exchange, this rate is a very sensitive probe of changes in the structure of a protein as well as of changes in

the dynamics (Wagner *et al.*, 1979b; Englander & Kallenbach, 1983).

Amide NH protons that exchange slowly (at pH 4.6 and 15 °C) with the solvent deuterons were identified from the assignments of the amide $C^{\alpha}H$–NH peaks observed in the DQF-COSY spectrum of des-[65–72]-RNase A dissolved in D_2O (a DQF-COSY spectrum obtained at pH 4.6 and 10 °C was used to confirm the existence of weak peaks in the spectrum obtained at the higher temperature). The following backbone amide protons of des-[65–72]-RNase A were found to be slowly exchanging: residues 9–11, 13, 14, 29–31, 43, 44, 46–49, 54–59, 73–75, 79, 81–85, 97, 98, 100, 102, 104, 106–111, 116, 118, and 119. All of the amide protons that exhibit a slow rate of exchange in des-[65–72]-RNase A at pH 4.6 at 15 °C also show a slow rate of exchange in native RNase A at pH 4.0 (Santoro *et al.*, 1993), presumably at 35 °C. A comparison with H/D exchange studies of native RNase A at pH 3.0 and 30 °C (Robertson *et al.*, 1989) shows that all of the slowly exchanging amide protons that are observed in des-[65–72]-RNase A are also observed in native RNase A, except for the amide protons of Asp-14 and Asp-83. The observed increase in the rate of amide H/D exchange at Asp-14 and Asp-83 in native RNase A at pH 3.0, compared to des-[65–72]-RNase A at pH 4.6, is probably due to the change in the local electrostatic field, as the side chains of Asp-14 and Asp-83 are expected to be fully protonated at pH 3.0 and only partially protonated at pH 4.6.

The following slowly exchanging backbone amide protons were observed in native RNase A, at pH 3.0 and 30 °C, but were not observed in the present study on des-[65–72]-RNase A: His-12, Gln-60 (we were unable to obtain assignments for Gln-60 in des-[65–72]-RNase A), Lys-61, Val-63, and Cys-72. (The five residues referred to above have slowly exchanging backbone amide protons in native RNase A at pH 4.0 and 35 °C.) These data show that the rupture of the disulfide bond involving residues Cys-65 and Cys-72 results in a local conformational change or increased flexibility involving the region comprising residues Gln-60–Cys-72 and that there is little change in the overall conformation of the protein. In fact, the amide protons of Tyr-73 and Gln-74 that are close to Cys-72 (in the sequence) are still slowly exchanging in des-[65–72]-RNase A; i.e., the amide protons of Tyr-73 and Gln-74 are not affected by rupture of the 65–72 disulfide bond.

His-12 is not close to this loop region that has been modified and yet it does not show any slowly exchanging amide protons, although both Gln-11 and Met-13 that are part of the same α-helix in RNase A do have slowly exchanging amide protons. This is either due to an intrinsically higher rate of H/D exchange in His-12 or due to conformational exchange in the vicinity of His-12. The absence of the *side-chain* $C^{\delta}H$–$C^{\epsilon}H$ cross peak of His-12 also suggests the existence of slow conformational change. In native RNase A, His-119 (known to be in the vicinity of His-12) adopts multiple conformations. Both His-119 and His-12 are part of the active site of RNase A. Therefore, other residues at the active site might also exhibit some flexibility. In the following section, we present evidence for conformational flexibility involving Val-43, a residue that is near other active-site residues, *viz.*, Lys-41 and Thr-45. In addition, we present evidence to show that either Thr-45 undergoes conformational change on the NMR time scale or the environment of Thr-45 changes on a millisecond time scale.

We offer a plausible mechanism to explain why rupture of the Cys-65–Cys-72 disulfide bond might bring about changes in the active site. In native RNase A, the backbone amide NH of Lys-66 forms a hydrogen bond with the side-chain carboxyl group of Asp-121 in solution as well in the crystalline state (Rico *et al.*, 1989, 1991). The rupture of the hydrogen bond involving Lys-66 and the active-site residue Asp-121 might be adequate to account for the small perturbations in the active site region of des-[65–72]-RNase A.

Effect of Solvent on Conformational Dynamics. The $C^{\beta}H$–$C^{\gamma}H$ cross peak of Thr-45 is found in the same region as the $C^{\beta}H$–$C^{\gamma}H$ cross peaks of valine residues in the DQF-COSY spectrum of des-[65–72]-RNase A in D_2O. However, this peak was not visible in the H_2O spectrum. The absence of the Thr-45 $C^{\beta}H$–$C^{\gamma}H$ cross peak in the H_2O spectrum is due either to a change in the mobility of Thr-45 or to mobility of a residue in the vicinity that affects the chemical shift of Thr-45. In either case, it is clear that replacement of D_2O by H_2O results in a change in the dynamic behavior of des-[65–72]-RNase A. This result is not entirely surprising. Changing the solvent from H_2O to D_2O results in an increase in the thermal stability of native RNase A (Hermans & Scheraga, 1959), due to changes in the zero-point vibrational energies of the relevant hydrogen bonds. Addition of acetate ion (1–5 mM) to the H_2O solution restores the missing $C^{\beta}H$–$C^{\gamma}H$ cross peaks of Thr-45 in the H_2O spectrum. Similar behavior was also observed for the $C^{\alpha}H$–NH cross peak of Thr-45 in the DQF-COSY spectrum of des-[65–72]-RNase A in H_2O. The $C^{\alpha}H$–NH cross peak of Thr-45 was observed in the DQF-COSY spectrum of des-[65–72]-RNase A in H_2O containing <10 mM acetic acid. However, the $C^{\alpha}H$–NH cross peak of Thr-45 was not visible in the DQF-COSY spectrum if the H_2O solution did not contain any acetic acid.

The $C^{\beta}H$–$C^{\gamma}H$ cross peaks of valine residues appear in a characteristic part of the DQF-COSY spectrum. For most of the valine residues, the two γ-methyl groups have different values of chemical shifts. Val-43 and Val-124, on the other hand, are the only two residues that have an identical value of the chemical shift for both of the γ-methyl groups. Introduction of a small concentration of acetate ion (1–5 mM acetic acid) into a solution of des-[65–72]-RNase A in H_2O results in the appearance of two γ-methyl resonances for Val-43, instead of the single resonance observed in the absence of the acetate ion. This shows that the binding of the acetate ion causes a change in the structure or flexibility of Val-43 or of residues in the vicinity that can affect its magnetic environment. We have not identified the binding site of acetate ion (or acetic acid) in this study. Acetic acid binds to native RNase A (Cann, 1971). Acetate (and propionate) ions probably bind to native RNase A in the vicinity of His-48 by means of hydrophobic interactions involving the alkyl group of the ligand (Tanokura, 1983).

However, although these data do not rule out the possibility that the effect of the acetate ion on des-[65–72]-RNase A is mediated through simple electrostatic interactions that are sensitive to the ionic strength of the solution, it appears more likely that the effect of the acetate ion is mediated by *binding* because the change in ionic strength of the solution was not extreme when a low concentration of acetate ion (<5 mM) was added (the solution was already 10–20 mM in NaCl as a result of adjusting the pH).

Comparison of the Chemical Shifts of Des-[65–72]-RNase A and RNase A. To compare the chemical shifts of the two proteins, we need to obtain assignments for both proteins at the same temperature and pH. The assignments for native RNase A have been carried out at pH 3.0 and 30 °C (Robertson *et al.*, 1989) and at pH 4.0 and 35 °C (Rico *et*

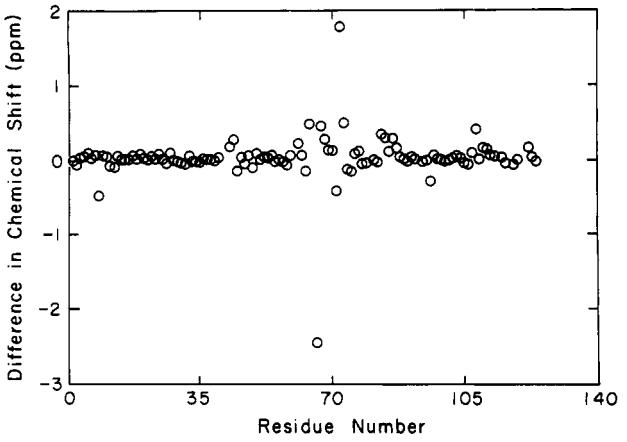

FIGURE 3: Plot of the chemical shift difference between the backbone amide NH's of RNase A and des-[65–72]-RNase A at pH 4.6 and 15 °C.

al., 1989). The assignments for des-[65–72]-RNase A were carried out at 20 °C and at 15 °C at pH 4.6, because des-[65–72]-RNase A is not stable at the lower pH and the higher temperature at which the assignments for native RNase A were obtained. Therefore, we obtained NOESY and TOCSY spectra of native RNase A at pH 4.6 and 15 °C. The chemical shifts of RNase A at pH 4.6 and 15 °C are expected to be similar to those at pH 3.0 and 30 °C. Therefore, it was not necessary to make a complete sequential resonance assignment for native RNase A at pH 4.6 and 15 °C. Well-resolved peaks in the spectrum of native RNase A were assigned first and then the remaining peaks were assigned by using sequential connectivities observed in the NOESY spectrum at pH 4.6 and 15 °C.

Figure 3 shows a plot of the chemical shift difference between the backbone amide NH's of RNase A and des-[65–72]-RNase A. A comparison of the chemical shifts of the amide NH protons in the two proteins showed that the amide NH chemical shifts in these two proteins are very similar. The chemical shift of the amide NH differs by more than 0.1 ppm for the following residues: 8, 43–45, 61, 63–75, 77, 83–87, 96, 108, 110, 111, and 122. The largest changes occur in residues 63–75. The other residues that exhibit chemical shift differences greater than 0.1 ppm for the amide NH's are located either close to residues 61–75 or close to active-site residues of native RNase A.

Regular Backbone Structure. The close similarity of the chemical shifts of native RNase A and those of des-[65–72]-RNase A, as well as the similarities in the H/D exchange behavior of des-[65–72]-RNase A and native RNase A, show that the regular backbone structure of des-[65–72]-RNase A is very similar to that of native RNase A.

The regular backbone structure of native RNase A (Wlodawer *et al.*, 1988) consists of three helices comprising residues 3–13, 24–34, and 50–60 and two antiparallel β-sheets. The first β-sheet consists of residues 41–48, 79–91, and 94–104 with a β-bulge at residues 88–89. The second β-sheet consists of residues 61–64, 71–75, 105–113, 114–119, and 121–124 (Wlodawer *et al.*, 1988). The pattern of NOE's and the pattern of slowly exchanging backbone amide protons showed that the structures of both β-sheets in des-[65–72]-RNase A are essentially the same as in native RNase A, except for minor differences involving residues 61–64. In native RNase A, the backbone amide proton of Val-63 exchanges slowly; however, we do not observe a slow rate of H/D exchange at Val-63 of des-[65–72]-RNase A and this suggests that conformational flexibility exists in this region of des-[65–72]-RNase A. Long-range $C^{\alpha}H$–$C^{\alpha}H$ NOE's involving residues Cys-72–Ala-109 and Gln-74–Ile-107, $C^{\alpha}H$–NH NOE's involving residues Cys-72–Cys-110 and Gln-74–Val-108, and NH–NH NOE's involving residues Tyr-73–Val-108 clearly show that residues 72–74 form one strand of the antiparallel sheet in des-[65–72]-RNase A.

Helix 1 of native RNase A consists of residues 3–13 (Wlodawer *et al.*, 1988). We observed medium-range NOE's involving residues 6–9, 7–10, 7–11, and 9–13, sequential NH–NH NOE's for residues 5–13, and slowly exchanging backbone amide hydrogens for residues 9–13. This clearly shows that the helix from residues 6 to 13 is preserved in des-[65–72]-RNase A. There is no evidence that residues 3–5 are in a helical conformation in des-[65–72]-RNase A. In native RNase A, Thr-3 is not helical and Ala-5 is helical (Robertson *et al.*, 1989; Rico *et al.*, 1989), and Ala-4 has been assigned as helical by Rico *et al.* (1989), but not by Robertson *et al.* (1989). Helix 2 of native RNase A consists of residues 23–33 (Wlodawer *et al.*, 1988). We found sequential NH–NH NOE's for residues 23–33 as expected for residues in a helical conformation. However, we found medium-range $C^{\alpha}H$–NH NOE's only for residues 26–29 and 29–33. Therefore, this helix is not as well-defined as in the X-ray structure of RNase A (Wlodawer *et al.*, 1988). This helix is also not very well defined in the solution structure of native RNase A (Rico *et al.*, 1989; Robertson *et al.*, 1989). Helix 3, involving residues 50–60 in native RNase A (Wlodawer *et al.*, 1988), shows sequential NH–NH NOE's from residues 51 to 58 and numerous i to $i + 3$ and i to $i + 4$ NOE's for residues 51–57. This shows that residues 51–57 are in a helical conformation, but we have no evidence that residues 59–60 are helical, as they are in the crystal structure (Wlodawer *et al.*, 1988). There is no evidence for helical structure involving residues 59 and 60 in the solution structure of intact RNase A (Robertson *et al.*, 1989; Rico *et al.*, 1989).

Stereospecific Assignments and Constraints for Side-Chain Dihedral Angles. Stereospecific assignments for the γ-methyl groups of valine were made by analyzing the data comprising $^3J_{C^{\alpha}H-C^{\beta}H}$ coupling constants and the intraresidue NOE's $C^{\alpha}H$–$C^{\beta}H$, $C^{\alpha}H$–$C^{\gamma}H$, NH–$C^{\beta}H$, and NH–$C^{\gamma}H$ and the sequential NOE's NH–$C^{\beta}H$ and NH–$C^{\gamma}H$ (Zuiderweg *et al.*, 1985; Hyberts *et al.*, 1987; Montelione *et al.*, 1992). This analysis was carried out by assuming that the side-chain conformation exists in one of three energetically favorable states, g^+, g^-, or t. A stereospecific assignment was made only if all of the data could be explained by the presence of a single side-chain conformation. Stereospecific assignments and constraints on the dihedral angle χ^1 were obtained for valines 47, 108, 116, and 118. A similar analysis of the $^3J_{C^{\alpha}H-C^{\beta}H}$ coupling constants, intraresidue NOE's, and sequential NOE's allowed us to obtain dihedral angle constraints for four of the 10 threonine residues, those at positions 78, 82, 99, and 100, and for Ile-107.

Assignment of NOE's. At the end of the sequential assignment process, almost all of the cross peaks involving NH, $C^{\alpha}H$, and $C^{\beta}H$ protons that were visible and resolved in the DQF-COSY spectrum were assigned. However, assignment of peaks in the NOESY spectrum was more difficult. For example, the amide NH's of Gly-88 and Asp-38 are degenerate at 15 °C. Hence, it was not possible to obtain unique assignments for any of the NOE peaks for which F_2 is 8.92. However, these peaks have slightly different temperature dependences of the chemical shift and are resolved at 20 °C, and this allowed us to assign the amide NH partner

of cross peaks that have F_2 = 8.92. Similarly, some cross peaks that could not be assigned at 20 °C due to overlaps could be assigned at 15 °C. We were able to obtain assignments for many NOESY peaks by iteratively going back and forth between the data sets acquired at 15 and at 20 °C. This procedure proved useful for the assignment of many NOE cross peaks that have an amide NH as a partner, because amide NH protons have a relatively large temperature dependence of their chemical shift.

There are many NOE's involving side-chain aromatic protons that could not be assigned by this procedure because the chemical shifts of side-chain aromatic protons have little or no dependence on temperature. We were able to obtain unique assignments for approximately 100 NOE's involving the aromatic side-chain protons of tyrosine, phenylalanine, and histidine residues by using the three-dimensional TOCSY–NOESY spectra.

Calibration of NOESY Data To Obtain Distance Bounds. NOESY spectra obtained by using a mixing time of 75 ms for H_2O and a mixing time of 100 ms for D_2O were used for calculating upper bounds for interproton distances. NOE's derived from the spectrum obtained in H_2O were calibrated by using the strongest sequential $C^{\alpha}H$–NH NOE's, which correspond to a distance of 2.2 Å by assuming a trans peptide group (Billeter *et al.*, 1982). NOE's involving protons that do not exchange with deuterons were calibrated by using the spectrum in D_2O. For these peaks, the fixed distance between the tyrosine $C^{\delta}H$ and $C^{\epsilon}H$ protons (1.8 Å) was used to calibrate the NOE intensities. NOE's involving geminal glycine $C^{\alpha}H$'s can also be used to calibrate the data in D_2O. However, we did not use the glycine $C^{\alpha}H$'s for calibration because these cross peaks were not as well resolved as the tyrosine $C^{\delta}H$–$C^{\epsilon}H$ cross peaks.

For all NOE's that did not involve a methyl group, the calibration was carried out by assuming that the intensity of the NOE cross peaks is proportional to $1/r^6$. This proportionality is strictly true only if the two protons are rigidly fixed with respect to each other in the molecule and if the molecule is undergoing isotropic rotational motion. Therefore, the rigid isotropic rotational model is not valid for NOE's involving methyl groups because the protons in a methyl group undergo rotational motion that is fast (Braun *et al.*, 1981) compared to the time scale for observation of NOE's. For NOE's involving methyl groups, the uniform averaging model was used to calibrate the NOE intensities (Woessner, 1962; Tropp, 1980; Braun *et al.*, 1981; Koning *et al.*, 1990). This model assumes that NOE intensity is proportional to $1/r^5$ and is a better model than the rigid-isotropic tumbling model for describing the observed distance dependence of NOE intensities involving methyl groups (Güntert *et al.*, 1991a).

Pseudoatom corrections were applied to distances involving methylene and methyl hydrogen atoms and to distances involving the aromatic hydrogens of tyrosine and phenylalanine (Wüthrich *et al.*, 1983; Güntert *et al.*, 1991a).

Application of Distance Geometry. The procedure described below was used to obtain a set of conformations that are consistent with the 485 interproton distance constraints derived from NOE data and the 28 dihedral angle constraints derived from measurements of coupling constants and analysis of NOE data. Random conformations were generated using the program DIANA (Güntert *et* al., 1991a), and initially, constraints between residues that are close to each other in the sequence were satisfied; constraints involving residues that are farther apart in the sequence were taken into account in subsequent steps, by mimimizing a variable target function. The minimization of the variable target function was also carried out with the program DIANA.

A total of 1260 random conformations were generated and the target function was minimized with the program DIANA. The root-mean-square (rms) deviations for all backbone atoms was computed for 17 of the structures with the lowest values of the target function. The range of backbone rms deviations for these 17 preliminary structures was 4.2–7.9 Å.

An examination of these structures showed that some of the constraints derived from the NMR data were violated. Many of these violations involved NOE's to the $C^{\delta}H$ of His-105 or to the $C^{\delta}H$ of His-119. Several NOE's involving His-119 and His-105 that appeared to be inconsistent with the existence of a *single* conformation were deleted from subsequent structural calculations. Multiple side-chain conformations for His-119 and His-105 are also seen in native RNase A—in solution (Rico *et al.*, 1989; Santoro *et al.*, 1993) as well as in crystals (Borkakoti *et al.*, 1982).

Redundant Dihedral Angle Constraints. An examination of the preliminary randomly generated structures obtained by using DIANA showed that some of the computed dihedral angles were constrained to a certain range, even though they were not explicitly constrained by the initial input data. These new constraints, which can then be used as additional input data, are referred to as redundant dihedral angle constraints and abbreviated as REDACs (Güntert & Wüthrich, 1991; Moy *et al.*, 1993). The use of REDACs derived from preliminary calculations of the complete structure can reduce the computation time for obtaining a group of acceptable conformers (Güntert & Wüthrich, 1991; Moy *et al.*, 1993).

To obtain a sufficient sampling of the conformational space, in addition to the 17 structures that were obtained from the first round of minimization of the target function, we carried out minimization of the variable target function, but only for the following *fragments* of des-[65–72]-RNase A (each one being treated individually) to generate a distribution of conformations that satisfied the constraints involving residues that are part of the fragment being considered: 5–20, 20–35, 35–50, 45–60, 79–104, 109–119, and 105–124. For the fragments 5–20, 20–35, and 45–60 (in which most of the residues adopt a helical conformation), 20 conformations that satisfied all of the constraints were obtained after minimization of 480 random conformations. However, for those fragments of des-[65–72]-RNase A that adopt a β-sheet conformation, it was necessary to use a larger number of conformations in order to obtain an acceptable number. For example, we found that it was necessary to minimize 4600 random conformations of the fragment 109–119 to obtain 16 structures that had acceptably low values of the target function. A new ensemble was constructed for *each* fragment by adding the conformations obtained by minimization of *individual* fragments to the original ensemble of 17 conformations obtained by minimization of the target function for the entire molecule. REDACs were identified for each separate fragment by using these new ensembles, for dihedral angles that are "well defined." A dihedral angle was considered to be well defined if the value of that dihedral angle was restricted to within 180° in all conformers in the ensemble that have low residual constraint violations.

The use of REDACS resulted in an increase in the ratio of the number of structures that converged to low values of the target function compared to the number of structures that were trapped in local minima. After minimization of another 462 random starting conformations using all of the constraints (the original constraints and REDACs), we were able to obtain

a set of 21 structures that satisfied most of the input constraints and had very few van der Waals overlaps. The average rms deviation for all backbone atoms of residues 5–124 was 5.4 Å (residues 1–4 were not well defined in this set of structures). This set of structures was superposed on the X-ray structure, and the rms deviations of the heavy atoms of des-[65–72]-RNase A from the corresponding atoms of the X-ray structure (Wlodawer *et al.*, 1988) ranged from 1.9 to 6.5 Å, and the average value of the rms deviations for the 21 structures was 5.1 Å for residues 5–124.

Assignment of NOE's Using Preliminary Models. The interpretation of two-dimensional NOESY data is limited by the fact that many cross peaks cannot be assigned to a unique pair of interacting spins because of chemical shift degeneracy. This problem was addressed by reinterpreting the NOESY spectra using the preliminary models of the structure described in the previous section. These structures were then used to interpret additional NOESY cross peaks for which one or both F_1 and F_2 resonance could not be assigned without structural information. If a proton pair was at a distance of greater than 6.5 Å in all eight of the best structures, then this pair was excluded from consideration. The 470 additional NOE's that could be assigned by using this procedure were added to the previous set. Approximately 1000 random starting conformations were used to generate new structures by minimizing the target function as described earlier. Nineteen of these conformations had a low value of the target function and were used to represent the solution structure of des-[65–72]-RNase A. The increased number of NOE's resulted in a substantial lowering of the rms deviation. The range of backbone rms deviation in these 19 structures was 2.14–5.36 Å, and the average of the rms deviations was 3.46 Å. For these 19 structures, the range of rms deviations from the X-ray structure was 2.62–4.69 Å and the average of the pairwise rms deviations from the X-ray structure was 3.51 Å.

Energy Minimization. The set of 19 structures described above was subjected to restrained energy minimization, using a method described in our earlier work on murine epidermal growth factor (Montelione *et al.*, 1992) and transforming growth factor α (Moy *et al.*, 1993). Restrained energy minimization was carried out by minimizing the function $F = \alpha f + (1 - \alpha)sE$, where f is the sum of squares of upper and steric constraint violations, E is the ECEPP/3 energy (Némethy *et al.*, 1992) with a minor modification that increases the weight for peptide bond planarity by a factor of 10 as described earlier (Moy *et al.*, 1993), and s was 1 mol Å^2/kcal and is needed because the ECEPP/3 energy and f have different units. α is a scaling factor determining the relative weights of the experimental constraints and ECEPP/3 energy. In this study, energy minimization was carried out in three steps. The relative weight for ECEPP/3 energy was gradually increased by using three different values of α, viz., 0.998, 0.987, and 0.833. The choice of the values for α is arbitrary.

Eight of the 19 structures attained low values of the function F, and the ϕ–ψ values of residues 5–124 for these eight structures are shown in Figure 4. An examination of the ϕ–ψ plot of the energy-minimized structures shows that, in these structures, ϕ and ψ are more restricted to energetically favorable regions compared to structures that had not been subjected to energy minimization (cf. Figure 5). In addition, the use of restrained energy minimization results in a substantial lowering of the energy without any significant violations of the input constraints.

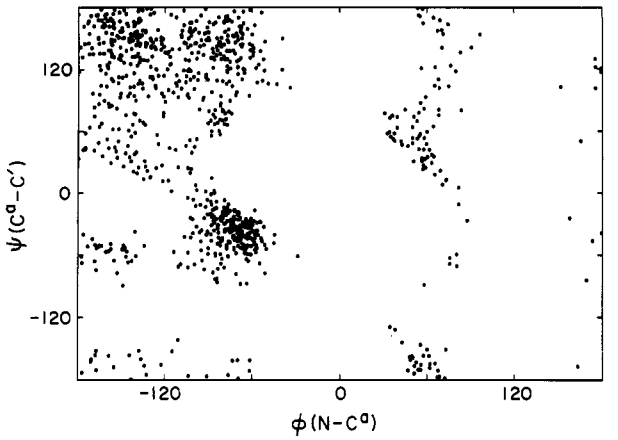

FIGURE 4: Distribution of ϕ and ψ for residues 5–124 in the final eight structures obtained by restrained energy minimization. Only non-glycine and non-proline residues are included.

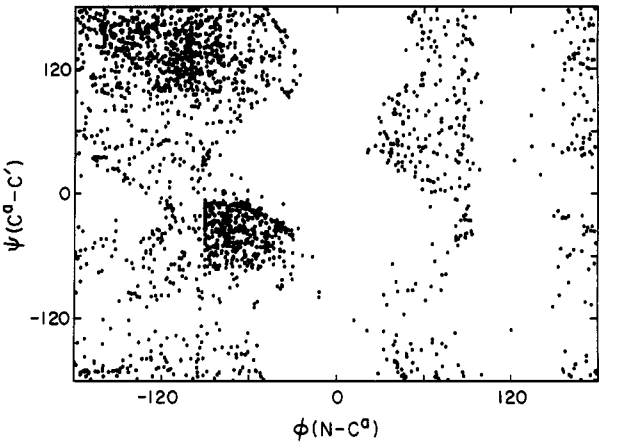

FIGURE 5: Distribution of ϕ and ψ for residues 5–124 in the 19 structures obtained by minimization of the target function after inclusion of the 470 additional NOE's obtained by reiterative interpretation of the NOE data. Only non-glycine and non-proline residues are included.

Table 3: Summary of Residual Constraint Violations for Final Eight Conformers of Des-[65–72]-RNase A

structure no.[a]	no. of upper bound constraint violations		no. of steric constraint violations[b]		no. of dihedral angle constraint violations	
	0.5–1.0 Å	>1.0 Å	0.1–0.3 Å	>0.3 Å	ϕ	χ^1
1	4	1	14	0	1	0
2	6	1	21	1	2	0
3	4	1	11	0	0	1
4	3	1	9	1	0	0
5	9	1	26	0	0	0
6	9	2	13	3	0	0
7	12	1	22	0	0	0
8	3	5	8	4	0	0

[a] The conformations obtained from restrained energy minimization were ordered so that the conformation with the lowest value of the target function is the first structure and the conformation with the highest value of the target function is the last. [b] A steric constraint violation occurs if the distance between the centers of two atoms is less than the sum of their van der Waals radii.

Table 3 shows the list of constraint violations and overlaps for the eight structures that converged during the restrained energy minimization. The range of backbone rms deviation (pairwise) in these eight structures for residues 5–124 was 2.61–4.96 Å, and the average of the rms (pairwise) deviation was 3.71 Å. For these eight structures, the range of rms deviations from the X-ray structure was 2.73–4.79 Å and the average of the rms deviations from the X-ray structure was

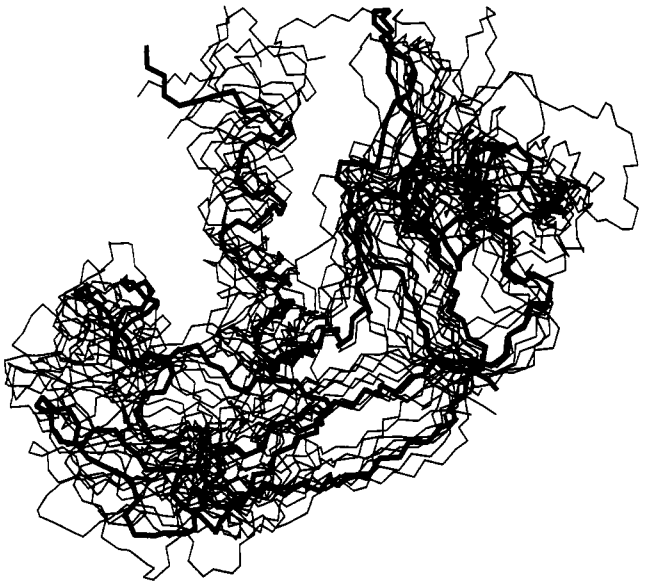

FIGURE 6: Superposition of the eight structures obtained by restrained energy minimization on that of the X-ray structure of native RNase A.

3.67 Å. The eight structures that attained low values of the function F were superposed on the X-ray structure of native RNase A (Wlodawer *et al.*, 1988). The superposition is displayed in Figure 6. The superposition reveals that the loop corresponding to residues 59–69 is the region of maximum variability (this loop is seen in the top right-hand corner of Figure 6). In the bottom left corner of Figure 6, three loops of high variability are seen. These are (from top to bottom) 36–40, 91–95, and 15–25. Of these three loops, the loop involving residues 91–95 is the most structurally variable, followed by the loop 36–40. Loop 15–25 is of moderate variability. Superposition of 80 core residues (these comprise approximately $^2/_3$ of the total number of residues in RNase A, with the following residues being excluded: 1–5, 15–19, 32–40, 60–70, 87–95, and 111–115) shows that the average of the pairwise backbone rms deviation of these eight conformers from the X-ray structure is 2.21 Å (range 1.77–2.50 Å). The rms deviation between the X-ray structure and the average structure (obtained by averaging the coordinates of the 80 core residues described above) is 1.53 Å.

Comparison with the Solution Structure of Native RNase A. The solution structure of native RNase A at pH 4.0 and 35 °C has been determined by using NMR spectroscopy (Rico *et al.*, 1991; Santoro *et al.*, 1993). They generated initial structures by using a biased sampling of the conformational space so that energetically favorable parts of the ϕ–ψ map were sampled preferentially. The target function for some of these segments was minimized separately to generate initial structures, and these fragments were subsequently merged together to yield eight structures. The rms differences for all backbone atoms between these eight structures ranged from 1.3 to 4.8 Å, and the range of rms differences from the X-ray structure was 1.8–3.4 Å (Rico *et al.*, 1991). In subsequent work (Santoro *et al.*, 1993), two structures obtained from an earlier study were subjected to further molecular dynamics to generate 16 structures, and these structures were refined by using the iterative relaxation matrix approach. The rms deviation between the *average* of these 16 structures and the X-ray structure was found to be 0.92 Å. These structures for native RNase A are considerably closer to each other and closer to the X-ray structure than the set of structures obtained for des-[65–72]-RNase A in this study.

Several factors contribute to the lower resolution in the structure determination of des-[65–72]-RNase A compared to that of native RNase A. Some of these factors are as follows: (1) The lower concentration of protein used to obtain the spectra leads to fewer NOE's. (2) The lower temperature used for the structure determination of des-[65–72]-RNase A (required to avoid denaturation) resulted in a broadening of the proton resonances and a consequent lowering of both sensitivity and resolution. (3) The higher value of the pH used in these studies of des-[65–72]-RNase A resulted in a higher rate of saturation transfer of the amide NH protons with the solvent water, giving rise to differences in the observed NOE intensities. It was necessary to use a higher pH because des-[65–72]-RNase A becomes denatured at lower pH. In addition, the increased flexibility of des-[65–72]-RNase A would also be expected to contribute to a lowering of the resolution of the structure determination.

However, qualitatively, the set of solution structures of native RNase A is similar to the set of solution structures of des-[65–72]-RNase A. In the set of structures of native RNase A, maximum deviations were reported for the loop regions 16–22, 34–38, 59–69, 87–91, and 114–116 (Rico *et al.*, 1991). These loop regions have particularly high rms deviations in the set of structures reported here. The β-sheet that includes residues 109–119 and 81–104 was well defined in native RNase A and also in des-[65–72]-RNase A.

CONCLUSION

The removal of the disulfide bond between residues Cys-65 and Cys-72 in native RNase A gives rise to an intermediate that has only minor differences in chemical shifts and in the distribution of slowly exchanging amide NH protons in all regions except residues 60–72. In addition, the catalytic activity of these two proteins is very similar. These data indicate that there are only minor structural differences between the two proteins. In spite of the close structural similarities between RNase A and des-[65–72]-RNase A, the thermal stability of des-[65–72]-RNase A is substantially lower. It appears that the primary cause of the loss of thermal stability is due to the lowering of the free energy of the unfolded state because of an increase in the entropy of the unfolded state of des-[65–72]-RNase A, as indicated by the thermal denaturation measurements and loop entropy calculations.

The close structural similarity between des-[65–72]-RNase A and RNase A suggests that no major conformational change is necessary for interconversion from one to the other. Therefore, in regeneration pathways that involve des-[65–72]-RNase A (regeneration of native RNase A from an unfolded and reduced state), the major conformational folding step occurs prior to or concurrently with the formation of des-[65–72]-RNase A. The final step in the regeneration pathway is therefore a *local* folding event involving structure formation in the loop extending from residues 60 to 72.

The low reactivity of Cys-65 and Cys-72 in des-[65–72]-RNase A with iodoacetate cannot be explained unambiguously because our NMR studies were carried out with des-[65–72]-RNase A in which the cysteines were blocked with cysteamine. However, we can offer a plausible explanation for the low reactivity. The NMR data show that, in des-[65–72]-RNase A, residues 72–74 and 107–109 form part of a larger antiparallel β-sheet. The formation of this antiparallel β-sheet creates a hydrophobic pocket, involving mainly residues Ile-107, Val-108, and Tyr-73. This hydrophobic pocket is also present in the X-ray structure of native RNase A (Wlodawer *et al.*, 1988). The side chain of Cys-72 is close

to this hydrophobic pocket and the free thiol of Cys-72 might be partially buried in this hydrophobic pocket, reducing its accessibility and accounting for the low reactivity of Cys-72 with iodoacetate. Presumably, local fluctuations make Cys-72 accessible to the much faster reacting AEMTS. We are unable to confirm this hypothesis with our NMR data because we were unable to obtain assignments for the cysteamine blocking groups of Cys-65 and Cys-72 in des-[65–72]-RNase A.

The most informative result of our structure determination in terms of insight into protein folding/unfolding is what it suggests about the reductive unfolding pathways of RNase A. In reduction pathways involving des-[65–72]-RNase A, the major conformational unfolding events occur during or after the further reduction of des-[65–72]-RNase A; i.e., des-[65–72]-RNase A is conformationally stable. In this regard, des-[65–72]-RNase A is similar to the intermediates of BPTI in which one of the native disulfides is reduced. All three of the native two-disulfide species of BPTI have nativelike structure and are not folding/unfolding intermediates in a structural sense (Staley & Kim, 1992). Furthermore, the reduction pathway of RNase A containing des-[65–72]-RNase A appears to be very similar to the reduction pathway of BPTI, in which the 14–38 disulfide is broken to form a two-disulfide protein with nativelike structure (Mendoza *et al.*, 1994). However, there is a major difference between the reduction pathways in these two proteins. In native BPTI, reduction of the 14–38 disulfide is 5 orders of magnitude faster than the subsequent reduction process to form a one-disulfide species (Creighton & Goldenberg, 1984; Mendoza *et al.*, 1994); i.e., the second step is rate determining, and there is considerable evidence to suggest that the rate-determining step in the reduction of BPTI involves *global* unfolding (Mendoza *et al.*, 1994). On the other hand, for RNase A, as discussed in the introduction, the reduction of the first disulfide bond (65–72 in the pathway discussed here) is rate-determining and, as indicated by the data presented here, appears to be a *local* unfolding process. This would suggest that the two proteins unfold by different mechanisms, i.e., global vs local unfolding.

These differences can be reconciled by a more general mechanism, particularly in light of recent studies of the reduction pathways of BPTI mutants (Mendoza et al., 1994), which suggest that the major (but not the sole) contributor to increasing the rate of reduction comes from mutations which decrease the conformational stability of the species being reduced. The first step in the reduction pathways of BPTI and RNase A (those pathways containing des-[65–72]-RNase A) involves local unfolding leading to the formation of stable nativelike intermediates. In the case of BPTI, the conformational stability of the intermediate is still high as indicated by the virtual identity in structure between the intermediate and the native protein (Naderi *et al.*, 1991) and the high activation barrier to subsequent reduction (Mendoza *et al.*, 1994). In the case of the reduction pathway of RNase A which involves des-[65–72]-RNase A, the initial local unfolding process that results in the reduction of the 65–72 disulfide bond leads to the conformational disruption of a large loop within the protein extending from residue 60 to 72, thereby accelerating the rate of the subsequent reduction step. However, the more rapid rate of reduction of des-[65–72]-RNase A relative to the native protein could reflect an acceleration in a second local unfolding event due to increased flexibility of des-[65–72]-RNase A, an increase in the stability of the transition state of other local unfolding events, or a decreased stability of des-[65–72]-RNase A such that a global unfolding reaction becomes favored, as suggested by comparison with the reduction process of BPTI. These possibilities cannot be differentiated from the data presented here, so that further study is necessary.

The results, however, do suggest that a local unfolding event is the first stage of protein reduction, which presumably serves to lower the barrier to subsequent reduction. Whether the initial local unfolding step is rate-determining will in all likelihood vary from one protein to another. It is important to recognize that the results presented here have provided information only about ground-state structures. While these results suggest that only a small structural perturbation is required for the inverconversion of RNase A and des-[65–72]-RNase A, it is possible that the transition state formed during that interconversion may involve considerably more disruption of structure than is observed in des-[65–72]-RNase A. Detailed kinetic studies are required to characterize the transition state.

ACKNOWLEDGMENTS

We thank Z. Zheng for providing us with a sample of des-[65–72]-RNase A that was used for some initial studies, V. G. Davenport for writing software for interfacing a Sun IPC computer to a Neslab RTE-110 bath to enable automation of the thermal transition measurements, Professors J. L. Markley and G. T. Montelione for allowing us to use their NMR spectrometers for some of the experiments, Biosym Technologies for providing us with the program Felix, Professor K. Wüthrich for providing us with the programs EASY and DIANA, K. D. Gibson for providing us with the program for restrained energy minimization, S. Rumsey for help with ECEPP/3 geometry, Pharmacia-LKB for the gift of a 2249 gradient pump, and Professor G. T. Montelione for helpful comments on the manuscript.

REFERENCES

Altmann, K.-H., & Scheraga, H. A. (1990) *J. Am. Chem. Soc. 112*, 4926.
Anfinsen, C. B., & Scheraga, H. A. (1975) *Adv. Protein Chem. 29*, 205.
Bax, A., & Davis, D. G. (1985) *J. Magn. Reson. 65*, 355.
Billeter, M., Braun, W., & Wüthrich, K. (1982) *J. Mol. Biol. 155*, 321.
Borkakoti, N., Moss, D. S., & Palmer, R. A. (1982) *Acta. Crystallogr. 38B*, 2210.
Brandts, J. F., & Hunt, L. (1967) *J. Am. Chem. Soc. 89*, 4826.
Braun, W., Bosch, C., Brown, L. R., Gō, N., & Wüthrich, K. (1981) *Biochim. Biophys. Acta 667*, 377.
Braunschweiler, L., & Ernst, R. R. (1983) *J. Magn. Reson. 53*, 521.
Bruice, T. W., & Kenyon, G. L. (1982) *J. Protein Chem. 1*, 47.
Cann, J. R. (1971) *Biochemistry 10*, 3713.
Cooper, A., Eyles, S. J., Radford, S. E., & Dobson, C. M. (1992) *J. Mol. Biol. 225*, 939.
Creighton, T. E. (1988) *Bioessays 8*, 57.
Creighton, T. E., & Goldenberg, D. P. (1984) *J. Mol. Biol. 179*, 497.
Darby, N. J., van Mierlo, C. P. M., Scott, G. H. E., Neuhaus, D., & Creighton, T. E. (1992) *J. Mol. Biol. 224*, 905.
Delepierre, M., Dobson, C. M., Karplus, M., Poulsen, F. M., States, D. J., & Wedin, R. E. (1987) *J. Mol. Biol. 197*, 111.
Denton, J. B., Konishi, Y., & Scheraga, H. A. (1982) *Biochemistry 21*, 5155.
Denton, M. E., & Scheraga, H. A. (1991) *J. Protein Chem. 10*, 213.
Doig, A. J., & Williams, D. H. (1991) *J. Mol. Biol. 217*, 389.
Eccles, C., Güntert, P., Billeter, M., & Wüthrich, K. (1991) *J. Biomol. NMR 1*, 111.

Englander, S. W., & Kallenbach, N. R. (1983) *Q. Rev. Biophys. 16*, 521.
Englander, S. W., & Wand, A. J. (1987) *Biochemistry 26*, 5953.
Goldenberg, D. P. (1992) *Trends Biochem. Sci. 17*, 257.
Griesinger, C., Sorensen, O. W., & Ernst, R. R. (1989) *J. Magn. Reson. 84*, 14.
Güntert, P., & Wüthrich, K. (1991) *J. Biomol. NMR 1*, 447.
Güntert, P., Braun, W., & Wüthrich, K. (1991a) *J. Mol. Biol. 217*, 517.
Güntert, P., Qian, Y. Q., Otting, G., Muller, M., Gehring, W., & Wüthrich, K. (1991b) *J. Mol. Biol. 217*, 531.
Hermans, J., & Scheraga, H. A. (1959) *Biochim. Biophys. Acta 36*, 534.
Hermans, J., Jr., & Scheraga, H. A. (1961) *J. Am. Chem. Soc. 83*, 3283.
Hurle, M. R., Eads, C. D., Pearlman, D. A., Seibel, G. L., Thomason, J., Kosen, P. A., Kollman, P., Anderson, S., & Kuntz, I. D. (1992) *Protein Sci. 1*, 91.
Hyberts, S. G., Marki, W., & Wagner, G. (1987) *Eur. J. Biochem. 164*, 625.
Jeener, J., Meier, B. H., Bachmann, P., & Ernst, R. R. (1979) *J. Chem. Phys. 71*, 4546.
Koning, T. M. G., Boelens, R., & Kaptein, R. (1990) *J. Magn. Reson. 90*, 111.
Konishi, Y., & Scheraga, H. A. (1980a) *Biochemistry 19*, 1308.
Konishi, Y., & Scheraga, H. A. (1980b) *Biochemistry 19*, 1316.
Konishi, Y., Ooi, T., & Scheraga, H. A. (1981) *Biochemistry 20*, 3945.
Konishi, Y., Ooi, T., & Scheraga, H. A. (1982a) *Biochemistry 21*, 4734.
Konishi, Y., Ooi, T., & Scheraga, H. A. (1982b) *Biochemistry 21*, 4741.
Konishi, Y., Ooi, T., & Scheraga, H. A. (1982c) *Proc. Natl. Acad. Sci. U.S.A. 79*, 5734.
Kosen, P. A. (1992) in *Stability of Protein Pharmaceuticals, Part A: Chemical and Physical Pathways of Protein Degradation* (Ahern, T. J., & Manning, M. C., Eds.) pp 31–67, Plenum Press, New York.
Kossiakoff, A. A. (1982) *Nature 296*, 713.
Kuroki, R., Inaki, K., Taniyama, Y., Kidokoro, S., Matsushima, M., Kikuchi, M., & Yutani, K. (1992) *Biochemistry 31*, 8323.
Lin, S. H., Konishi, Y., Denton, M. E., & Scheraga, H. A. (1984) *Biochemistry 23*, 5504.
Ludvigsen, S., Andersen, K. V., & Poulsen, F. M. (1991) *J. Mol. Biol. 217*, 731.
Macura, S., & Ernst, R. R. (1980) *Mol. Phys. 41*, 95.
Matthew, J. B., & Richards, F. M. (1983) *J. Biol. Chem. 258*, 3039.
Mendoza, J. A., Jarstfer, M. B., & Goldenberg, D. P. (1994) *Biochemistry 33*, 1143.
Milburn, P. J., & Scheraga, H. A. (1988) *J. Protein Chem. 7*, 377.
Montelione, G. T., Wüthrich, K., Burgess, A. W., Nice, E. C., Wagner, G., Gibson, K. D., & Scheraga, H. A. (1992) *Biochemistry 31*, 236.
Moy, F. J., Li. Y.-C., Rauenbuehler, P., Winkler, M. E., Scheraga, H. A., & Montelione, G. T. (1993) *Biochemistry 32*, 7334.
Naderi, H. M., Thomason, J. F., Borgias, B. A., Anderson, S., James, T. L., & Kuntz, I. D. (1991) In *Conformations and Forces in Protein Folding* (Nall, B. T., & Dill, K. A., Eds.) pp 86–114, American Association for the Advancement of Science, Washington, DC.
Némethy, G., Gibson, K. D., Palmer, K. A., Yoon, C. N., Paterlini, G., Zagari, A., Rumsey, S., & Scheraga, H. A. (1992) *J. Phys. Chem. 96*, 6472.
Neuhaus, D., Wagner, G., Vasak, M., Kagi, H. R., & Wüthrich, K. (1985) *Eur. J. Biochem. 151*, 257.
Oschkinat, H., Cieslar, C., Gronenborn, A. M., & Clore, G. M. (1989) *J. Magn. Reson. 81*, 212.
Pace, C. N., Grimsley, G. R., Thomson, J. A., & Barnett, B. J. (1988) *J. Biol. Chem. 263*, 11820.
Piantini, U., Sørensen, O. W., & Ernst, R. R. (1982), *J. Am. Chem. Soc. 104*, 6800.
Poland, D. C., & Scheraga, H. A. (1965) *Biopolymers 3*, 379.
Privalov, P. L., Tiktopulo, E. I., & Khechinashvili, N. N. (1973) *Int. J. Pept. Protein Res. 5*, 229.
Redfield, A. G., & Kunz, S. D. (1975) *J. Magn. Reson. 19*, 250.
Richards, F. M. (1979) *Carlsberg Res. Commun. 44*, 47.
Richardson, J. S. (1981) *Adv. Protein Chem. 34*, 167.
Rico, M., Bruix, M., Santoro, J., Gonzalez, C., Neira, J. L., Nieto, J. L., & Herranz, J. (1989) *Eur. J. Biochem. 183*, 623.
Rico, M., Santoro, J., Gonzalez, C., Bruix, M., Neira, J. L., Nieto, J. L., & Herranz, J. (1991) *J. Biomol. NMR 1*, 283.
Robertson, A. D., Purisima, E. O., Eastman, M. A., & Scheraga, H. A. (1989) *Biochemistry 28*, 5930.
Rothwarf, D. M., & Scheraga, H. A. (1991) *J. Am. Chem. Soc. 113*, 6293.
Rothwarf, D. M., & Scheraga, H. A. (1992) *Proc. Natl. Acad. Sci. U.S.A. 89*, 7944.
Rothwarf, D. M., & Scheraga, H. A. (1993a) *Biochemistry 32*, 2671.
Rothwarf, D. M., & Scheraga, H. A. (1993b) *Biochemistry 32*, 2680.
Rothwarf, D. M., & Scheraga, H. A. (1993c) *Biochemistry 32*, 2690.
Rothwarf, D. M., & Scheraga, H. A. (1993d) *Biochemistry 32*, 2698.
Santoro, J., Gonzalez, C., Bruix, M., Neira, J. L., Nieto, J. L., Herranz, J., & Rico, M. (1993) *J. Mol. Biol. 229*, 722.
Scheraga, H. A., Konishi, Y., & Ooi, T. (1984) *Adv. Biophys. 18*, 21.
Schultz, D. A., Schmid, F. X., & Baldwin, R. L. (1992) *Protein Sci. 1*, 917.
Scott, R. A., & Scheraga, H. A. (1963) *J. Am. Chem. Soc. 85*, 3866.
Staley, J. P., & Kim, P. S. (1992) *Proc. Natl. Acad. Sci. U.S.A. 89*, 1519.
Tanokura, M. (1983) *J. Biochem. (Tokyo) 94*, 51.
Thornton, J. M. (1981) *J. Mol. Biol. 151*, 261.
Tiktopulo, E. I., & Privalov, P. L. (1974) *Biophys. Chem. 1*, 349.
Tropp, J. (1980) *J. Chem. Phys. 72*, 6035.
Tsong, T. Y., Hearn, R. P., Wrathall, D. P., & Sturtevant, J. M. (1970) *Biochemistry 9*, 2666.
Tüchsen, E., & Woodward, C. (1985) *J. Mol. Biol. 185*, 405.
van Mierlo, C. P. M., Darby, N. J., Neuhaus, D., & Creighton, T. E. (1991) *J. Mol. Biol. 222*, 353.
van Mierlo, C. P. M., Darby, N. J., Keeler, J., Neuhaus, D., & Creighton, T. E. (1993) *J. Mol. Biol. 229*, 1125.
Wagner, G., (1983) *Q. Rev. Biophys. 16*, 1.
Wagner, G., Kalb, A. J., & Wüthrich, K. (1979a) *Eur. J. Biochem. 95*, 249.
Wagner, G., Tschesche, H., & Wüthrich, K. (1979b) *Eur. J. Biochem. 95*, 239.
Wang, M. C., & Uhlenbeck, G. E. (1945) *Rev. Mod. Phys. 17*, 323.
Wlodawer, A., Svensson, L. A., Sjölin, L., & Gilliland, G. L. (1988) *Biochemistry 27*, 2705.
Woessner, D. E. (1962) *J. Chem. Phys. 36*, 1.
Wüthrich, K. (1986) *NMR of Proteins and Nucleic Acids*, pp 14–19 and 130–161, Wiley, New York.
Wüthrich, K., Wider, G., Wagner, G., & Braun, W. (1982) *J. Mol. Biol. 155*, 311.
Wüthrich, K., Billeter, M., & Braun, W. (1983) *J. Mol. Biol. 169*, 949.
Wüthrich, K., Billeter, M., & Braun, W. (1984) *J. Mol. Biol. 180*, 715.
Zuiderweg, E. R. P., Boelens, R., & Kaptein, R. (1985) *Biopolymers 24*, 601.